GT-PML: Generalized Theory of Perfectly Matched Layers and Its Application to the Reflectionless Truncation of Finite-Difference Time-Domain Grids

Li Zhao, *Member, IEEE,* and Andreas C. Cangellaris, *Member, IEEE*

***Abstract*— A new mathematical formulation is presented for the systematic development of perfectly matched layers from Maxwell's equations in properly constructed anisotropic media. The proposed formulation has an important advantage over the original Berenger's perfectly matched layer in that it can be implemented in the time domain without any splitting of the fields. The details of the numerical implementation of the proposed perfectly matched absorbers in the context of the finite-difference time-domain approximation of Maxwell's equations are given. Results from three-dimension (3-D) simulations are used to illustrate the effectiveness of the media constructed using the proposed approach as absorbers for numerical grid truncation.**

I. Introduction

SINCE THE original work by Berenger [1], the concept of perfectly matched layers (PML's) for reflectionless absorption of electromagnetic fields and its implementation for numerical grid truncation in both time-domain and frequency-domain wave simulations using finite methods has become the focus of extensive research [2]–[12]. Among the various implementations of PML's, the one by Sacks *et al.* [9] appears very attractive in view of the fact that its construction is based on the use of anisotropic media. Thus Maxwell's equations maintain their familiar physical form (except for the strange properties of the constructed anisotropic medium). Recently, it was shown that the (apparently nonphysical) Chew–Weedon formulation of PML's using a modified Maxwell's system with complex coordinate stretching [2], can be made equivalent to the anisotropic medium approach of [9] with an appropriate scaling of the involved electric and magnetic fields [13].

While both the anisotropic medium formulation and the formulation based on the modification of Maxwell's equations with complex coordinate stretching [2], [7] provide for a convenient implementation of PML's in frequency-domain finite element and finite difference modeling, their time-domain implementations in the context of the finite-difference time-domain (FDTD) method require the splitting of the fields, similarly with Berenger's original PML formulation. Recently, Mittra and Pekel [8] and Veihl and Mittra [10] have proposed and attempted an alternative formulation of Berenger's scheme where the splitting of the field components is avoided. Instead, time- and field-dependent sources are introduced. As suggested in [13], an unsplit-field implementation of PML's in the time domain can also be effected directly from the anisotropic medium formulation of the PML.

In this paper, we generalize the formulation proposed in [13] and, thus, establish a systematic procedure for the development of anisotropic media PML's that can be implemented for the truncation of FDTD grids without splitting of the fields. The proposed formulation is different from the one presented recently by Gedney [15], in terms of both the mathematical development of the time-dependent form of Maxwell's equations inside the PML medium and its numerical implementation in the FDTD algorithm. In Section II, the mathematical formulation is presented for the construction of the permittivity and permeability tensors of the anisotropic PML in order to effect a reflectionless planar interface. The construction of absorbing PML's for grid truncation in three dimensions is presented in Section III. Section IV includes the details of the numerical implementation of the absorbing PML's in the FDTD algorithm without splitting of the fields. In Section V, numerical examples are given from transient radiation problems in order to demonstrate the validity of the proposed formulation and compare its performance and accuracy with that of the split-field implementation. Section VI concludes the presentation with a summary of the attributes of the proposed generalized theory of perfectly matched layers (GT-PML).

II. The GT-PML Theory

With the assumption of a time dependence of the form $e^{j\omega t}$, Maxwell's equations in an anisotropic medium have the form

$$\nabla \times \boldsymbol{E} = -j\omega\overline{\mu} \cdot \boldsymbol{H} \tag{1a}$$

$$\nabla \times \boldsymbol{H} = j\omega\overline{\epsilon} \cdot \boldsymbol{E} \tag{1b}$$

$$\nabla \cdot (\overline{\epsilon} \cdot \boldsymbol{E}) = 0 \tag{1c}$$

$$\nabla \cdot (\overline{\mu} \cdot \boldsymbol{H}) = 0 \tag{1d}$$

where $\overline{\mu}$ and $\overline{\epsilon}$ are respectively the permeability and permittivity tensors of the medium. Motivated by the results in [9], the two tensors are assumed to be of the form

$$\overline{\epsilon} = \epsilon(\mathrm{diag}\,\{a_x, a_y, a_z\}) = \epsilon[\Lambda] \tag{2a}$$

$$\overline{\mu} = \mu(\mathrm{diag}\,\{a_x, a_y, a_z\}) = \mu[\Lambda] \tag{2b}$$

Manuscript received March 29, 1996.

The authors are with the Electromagnetics Laboratory, Department of Electrical and Computer Engineering, University of Arizona, Tucson, AZ 85721 USA.

Publisher Item Identifier S 0018-9480(96)08558-4.

where the elements of the diagonal matrix

$$[\Lambda] = \text{diag}\,\{a_x, a_y, a_z\} \tag{3}$$

are, in general, complex, dimensionless, constants.

Next, the *scaled* fields $\hat{\boldsymbol{E}}$ and $\hat{\boldsymbol{H}}$ are defined as follows:

$$\{\hat{E}_x, \hat{E}_y, \hat{E}_z\}^T = [G]^{-1}\{E_x, E_y, E_z\}^T \tag{4a}$$
$$\{\hat{H}_x, \hat{H}_y, \hat{H}_z\}^T = [G]^{-1}\{H_x, H_y, H_z\}^T \tag{4b}$$

where the superscript T denotes matrix transposition and

$$[G] = \text{diag}\,\{g_x, g_y, g_z\} \tag{5}$$

where g_x, g_y, g_z are, in general, complex constants. Using the notation $\overline{\boldsymbol{G}}$ and $\overline{\boldsymbol{\Lambda}}$ to denote the tensors with matrix representations $[G]$ and $[\Lambda]$, respectively, Maxwell's equations can be written in terms of the scaled fields $\hat{\boldsymbol{E}}$ and $\hat{\boldsymbol{H}}$

$$\nabla \times (\overline{\boldsymbol{G}} \cdot \hat{\boldsymbol{E}}) = -j\omega\mu\overline{\boldsymbol{\Lambda}} \cdot \overline{\boldsymbol{G}} \cdot \hat{\boldsymbol{H}} \tag{6a}$$
$$\nabla \times (\overline{\boldsymbol{G}} \cdot \hat{\boldsymbol{H}}) = j\omega\epsilon\overline{\boldsymbol{\Lambda}} \cdot \overline{\boldsymbol{G}} \cdot \hat{\boldsymbol{E}} \tag{6b}$$
$$\nabla \cdot (\epsilon\overline{\boldsymbol{\Lambda}} \cdot \overline{\boldsymbol{G}} \cdot \hat{\boldsymbol{E}}) = 0 \tag{6c}$$
$$\nabla \times (\mu\overline{\boldsymbol{\Lambda}} \cdot \overline{\boldsymbol{G}} \cdot \hat{\boldsymbol{H}}) = 0. \tag{6d}$$

It was shown in [13] that a choice of the scaling factors g_x, g_y, g_z according to the equations

$$\left(\frac{g_x}{g_y}\right)^2 = \frac{a_y}{a_x}, \quad \left(\frac{g_y}{g_z}\right)^2 = \frac{a_z}{a_y}, \quad \left(\frac{g_z}{g_x}\right)^2 = \frac{a_x}{a_z} \tag{7}$$

allows us to cast the system of (6) in the following form

$$\nabla_{\boldsymbol{a}} \times \hat{\boldsymbol{E}} = -j\omega\mu\hat{\boldsymbol{H}} \tag{8a}$$
$$\nabla_{\boldsymbol{a}} \times \hat{\boldsymbol{H}} = j\omega\epsilon\hat{\boldsymbol{E}} \tag{8b}$$
$$\nabla_{\boldsymbol{a}} \cdot (\epsilon\hat{\boldsymbol{E}}) = 0 \tag{8c}$$
$$\nabla_{\boldsymbol{a}} \cdot (\mu\hat{\boldsymbol{H}}) = 0 \tag{8d}$$

where

$$\nabla_{\boldsymbol{a}} \stackrel{\text{def}}{=} \hat{\boldsymbol{x}}\frac{1}{\sqrt{a_y a_z}}\partial_x + \hat{\boldsymbol{y}}\frac{1}{\sqrt{a_z a_x}}\partial_y + \hat{\boldsymbol{z}}\frac{1}{\sqrt{a_x a_y}}\partial_z. \tag{9}$$

The system in (8) is reminiscent of the modified Maxwell's system with complex coordinate stretching used in [2]. Indeed, using the notation

$$s_x = \sqrt{a_y a_z}, \quad s_y = \sqrt{a_z a_x}, \quad s_z = \sqrt{a_x a_y} \tag{10}$$

the system in (8) becomes mathematically equivalent with the modified Maxwell's system in [2]. However, there is an important difference. The system in (8) is for the scaled electric and magnetic fields while the one in [2] was proposed assuming that the fields are physical fields. Thus, as pointed out in [13], the complex coordinate stretching formulation of perfectly matched layers can be considered as an alternative representation of Maxwell's equations in an anisotropic medium only if the fields on which the modified ∇ operator operates are a scaled version of the physical fields as defined in (4).

The next step involves the investigation of the dispersion properties of this anisotropic medium. For this purpose, consider a general plane wave with scaled fields

$$\hat{\boldsymbol{E}} = \overline{\boldsymbol{G}}^{-1} \cdot \boldsymbol{E} = \hat{\boldsymbol{E}}_{\boldsymbol{0}} \exp(-j\boldsymbol{k} \cdot \boldsymbol{r}) \tag{11a}$$
$$\hat{\boldsymbol{H}} = \overline{\boldsymbol{G}}^{-1} \cdot \boldsymbol{H} = \hat{\boldsymbol{H}}_{\boldsymbol{0}} \exp(-j\boldsymbol{k} \cdot \boldsymbol{r}) \tag{11b}$$

where $\boldsymbol{k} = \hat{\boldsymbol{x}}k_x + \hat{\boldsymbol{y}}k_y + \hat{\boldsymbol{z}}k_z$. Substituting (11a,b) in the system (8) above, and using the fact that the medium is assumed to be homogeneous, one obtains

$$\boldsymbol{k_s} \times \hat{\boldsymbol{E}} = \omega\mu\hat{\boldsymbol{H}} \tag{12a}$$
$$\boldsymbol{k_s} \times \hat{\boldsymbol{H}} = -\omega\epsilon\hat{\boldsymbol{E}} \tag{12b}$$
$$\boldsymbol{k_s} \cdot \hat{\boldsymbol{E}} = 0 \tag{12c}$$
$$\boldsymbol{k_s} \cdot \hat{\boldsymbol{H}} = 0 \tag{12d}$$

where

$$\boldsymbol{k_s} = \hat{\boldsymbol{x}}\frac{k_x}{s_x} + \hat{\boldsymbol{y}}\frac{k_y}{s_y} + \hat{\boldsymbol{z}}\frac{k_z}{s_z}. \tag{13}$$

Eliminating $\hat{\boldsymbol{H}}$ between (12a) and (12b) results in

$$\boldsymbol{k_s} \times \boldsymbol{k_s} \times \hat{\boldsymbol{E}} = -\omega^2\mu\epsilon\hat{\boldsymbol{E}}$$

or

$$(\boldsymbol{k_s} \cdot \boldsymbol{k_s})\hat{\boldsymbol{E}} - (\boldsymbol{k_s} \cdot \hat{\boldsymbol{E}})\boldsymbol{k_s} = \omega^2\mu\epsilon\hat{\boldsymbol{E}}$$

and, finally, in view of (12c) and (13)

$$\omega^2\mu\epsilon = \frac{k_x^2}{s_x^2} + \frac{k_y^2}{s_y^2} + \frac{k_z^2}{s_z^2}. \tag{14}$$

Equation (14) is the dispersion relation for the anisotropic medium under study. It is satisfied by

$$k_x = ks_x \sin\theta\cos\phi \tag{15a}$$
$$k_y = ks_y \sin\theta\sin\phi \tag{15b}$$
$$k_z = ks_z \cos\theta \tag{15c}$$

where $k = \omega\sqrt{\mu\epsilon}$. Clearly, the propagation characteristics of the wave along x, y and z can be controlled by varying s_x, s_y and s_z or, effectively, (in view of (10)) by varying the properties of the anisotropic medium. In the following, the relationship between the tensors of two anisotropic media separated by a planar interface will be established for the interface to be reflectionless for all angles of incidence and all frequencies.

Without loss of generality the planar interface is taken to coincide with the $z = 0$ plane in a Cartesian coordinate system. The space $z < 0$ (Medium 1) is filled with a homogeneous medium with tensors $\epsilon_1[\Lambda_1], \mu_1[\Lambda_1]$, where $[\Lambda_1] = \text{diag}\,\{a_{1x}, a_{1y}, a_{1z}\}$, and corresponding s_{1x}, s_{1y} and s_{1z} values given by (10). The space $z > 0$ (Medium 2) is filled with a homogeneous medium with tensors $\epsilon_2[\Lambda_2], \mu_2[\Lambda_2]$, where $[\Lambda_2] = \text{diag}\,\{a_{2x}, a_{2y}, a_{2z}\}$, and corresponding s_{2x}, s_{2y} and s_{2z} values given by (10). A plane wave propagating from Medium 1 toward Medium 2 is assumed to be obliquely incident on the interface at $z = 0$. Its polarization is assumed arbitrary, and the standard decomposition of the field in its transverse electric to z (TE_z) and transverse magnetic to

z (TM_z) parts is used for the purposes of studying the reflection properties of the interface.

Concentrating first on the TE_z part of the wave (i.e. the electric field has components on the xy plane only), let

$$\boldsymbol{E_i} = \boldsymbol{E_0} e^{-\jmath \boldsymbol{k_i}\cdot\boldsymbol{r}} \tag{16a}$$

be the incident electric field, with corresponding scaled field

$$\hat{\boldsymbol{E}}_{\boldsymbol{i}} = \overline{\boldsymbol{G_1}}^{-1} \cdot \boldsymbol{E_i} = \hat{\boldsymbol{E}}_{\boldsymbol{0}} e^{-\jmath \boldsymbol{k_i}\cdot\boldsymbol{r}} \tag{16b}$$

where $\hat{\boldsymbol{E}}_{\boldsymbol{0}} = \overline{\boldsymbol{G_1}}^{-1} \cdot \boldsymbol{E_0}$ and the tensor $\overline{\boldsymbol{G_1}}$ has the matrix representation

$$[G_1] = \mathrm{diag}\,\{g_{1x}, g_{1y}, g_{1z}\}.$$

The corresponding scaled magnetic field is obtained from (12a)

$$\hat{\boldsymbol{H}}_{\boldsymbol{i}} = \frac{\boldsymbol{k_{is}} \times \hat{\boldsymbol{E}}_{\boldsymbol{0}}}{\omega\mu_1} e^{-\jmath \boldsymbol{k_i}\cdot\boldsymbol{r}}. \tag{16c}$$

In the above equations, $\boldsymbol{k_{is}}$ is (according to (13))

$$\boldsymbol{k_{is}} = \hat{\boldsymbol{x}}\frac{k_{ix}}{s_{1x}} + \hat{\boldsymbol{y}}\frac{k_{iy}}{s_{1y}} + \hat{\boldsymbol{z}}\frac{k_{iz}}{s_{1z}}.$$

The reflected electric field is written as

$$\boldsymbol{E_r} = R^{\mathrm{TE}} \boldsymbol{E_0} e^{-\jmath \boldsymbol{k_r}\cdot\boldsymbol{r}} \tag{17a}$$

with corresponding scaled field

$$\hat{\boldsymbol{E}}_{\boldsymbol{r}} = \overline{\boldsymbol{G_1}}^{-1} \cdot \boldsymbol{E_r} = R^{\mathrm{TE}} \hat{\boldsymbol{E}}_{\boldsymbol{0}} e^{-\jmath \boldsymbol{k_r}\cdot\boldsymbol{r}}. \tag{17b}$$

The corresponding scaled magnetic field is

$$\hat{\boldsymbol{H}}_{\boldsymbol{r}} = R^{\mathrm{TE}} \frac{\boldsymbol{k_{rs}} \times \hat{\boldsymbol{E}}_{\boldsymbol{0}}}{\omega\mu_1} e^{-\jmath \boldsymbol{k_r}\cdot\boldsymbol{r}}. \tag{17c}$$

The expression for $\boldsymbol{k_{rs}}$ is similar to the one for $\boldsymbol{k_{is}}$ given above.

Finally, the transmitted electric field is written as

$$\boldsymbol{E_t} = \boldsymbol{E_{0t}} e^{-\jmath \boldsymbol{k_t}\cdot\boldsymbol{r}} \tag{18a}$$

with corresponding scaled field

$$\hat{\boldsymbol{E}}_{\boldsymbol{t}} = \overline{\boldsymbol{G_2}}^{-1} \cdot \boldsymbol{E_t} = \hat{\boldsymbol{E}}_{\boldsymbol{0t}} e^{-\jmath \boldsymbol{k_t}\cdot\boldsymbol{r}} \tag{18b}$$

where $\hat{\boldsymbol{E}}_{\boldsymbol{0t}} = \overline{\boldsymbol{G_2}}^{-1} \cdot \boldsymbol{E_{0t}}$ and the tensor $\overline{\boldsymbol{G_2}}$ has the matrix representation

$$[G_2] = \mathrm{diag}\,\{g_{2x}, g_{2y}, g_{2z}\}.$$

The corresponding scaled magnetic field is

$$\hat{\boldsymbol{H}}_{\boldsymbol{t}} = \frac{\boldsymbol{k_{ts}} \times \hat{\boldsymbol{E}}_{\boldsymbol{0t}}}{\omega\mu_2} e^{-\jmath \boldsymbol{k_t}\cdot\boldsymbol{r}} \tag{18c}$$

where the expression for $\boldsymbol{k_{ts}}$ is similar to the one for $\boldsymbol{k_{is}}$ given above.

Boundary conditions at the interface involve the tangential components of the physical fields. First of all, from phase matching requirements one obtains $k_{ix} = k_{rx} = k_{tx}$ and $k_{iy} = k_{ry} = k_{ty}$. With this result in hand, the boundary conditions at $z = 0$ are as follows. From the continuity of the tangential physical electric field

$$(1 + R^{\mathrm{TE}})\overline{\boldsymbol{G_1}} \cdot \hat{\boldsymbol{E}}_{\boldsymbol{0}} = \overline{\boldsymbol{G_2}} \cdot \hat{\boldsymbol{E}}_{\boldsymbol{0t}} \tag{19}$$

and the continuity of the tangential components of the physical magnetic field the following two scalar equations result

$$\frac{(1 - R^{\mathrm{TE}})k_{1z}}{\omega\mu_1 s_{1z}} g_{1x} \hat{E}_{0y} = \frac{k_{2z}}{\omega\mu_2 s_{2z}} g_{2x} \hat{E}_{0ty}$$
$$\frac{(1 - R^{\mathrm{TE}})k_{1z}}{\omega\mu_1 s_{1z}} g_{1y} \hat{E}_{0x} = \frac{k_{2z}}{\omega\mu_2 s_{2z}} g_{2y} \hat{E}_{0tx}$$

where the fact that $k_{rz} = -k_{iz}$ has been used along with the change of notation $k_{iz} = k_{1z}$ and $k_{tz} = k_{2z}$. Actually, the last two equations may be cast in a form that involves only the physical fields using the fact that $E_{0x} = g_{1x}\hat{E}_{0x}, E_{0y} = g_{1y}\hat{E}_{0y}, E_{0tx} = g_{2x}\hat{E}_{0tx}$ and $E_{0ty} = g_{2y}\hat{E}_{0ty}$. If we also set

$$\boldsymbol{E_{0t}} = T^{\mathrm{TE}} \boldsymbol{E_0}$$

the resulting equations are

$$\frac{(1 - R^{\mathrm{TE}})k_{1z}}{\omega\mu_1 s_{1z}} \frac{g_{1x}}{g_{1y}} E_{0y} = \frac{k_{2z}}{\omega\mu_2 s_{2z}} \frac{g_{2x}}{g_{2y}} T^{\mathrm{TE}} E_{0y} \tag{20a}$$
$$\frac{(1 - R^{\mathrm{TE}})k_{1z}}{\omega\mu_1 s_{1z}} \frac{g_{1y}}{g_{1x}} E_{0x} = \frac{k_{2z}}{\omega\mu_2 s_{2z}} \frac{g_{2y}}{g_{2x}} T^{\mathrm{TE}} E_{0x}. \tag{20b}$$

Clearly, the identity obtained from (20)

$$\frac{g_{1x}}{g_{1y}} = \frac{g_{2x}}{g_{2y}} \tag{21}$$

reduces (20a) and (20b) to the same equation

$$k_{1z}\mu_2 s_{2z}(1 - R^{\mathrm{TE}}) = k_{2z}\mu_1 s_{1z} T^{\mathrm{TE}}. \tag{22}$$

From (19), (20) and (21) the expression for the reflection coefficient is obtained

$$R^{\mathrm{TE}} = \frac{k_{1z}\mu_2 s_{2z} - k_{2z}\mu_1 s_{1z}}{k_{1z}\mu_2 s_{2z} + k_{2z}\mu_1 s_{1z}}. \tag{23}$$

A similar procedure can be applied to obtain the reflection coefficient, R^{TM} for the TM_z part of the wave. The resulting expression is

$$R^{\mathrm{TM}} = \frac{k_{1z}\epsilon_2 s_{2z} - k_{2z}\epsilon_1 s_{1z}}{k_{1z}\epsilon_2 s_{2z} + k_{2z}\epsilon_1 s_{1z}}. \tag{24}$$

At this point, it is appropriate to recall the phase matching conditions

$$\omega\sqrt{\mu_1\epsilon_1}\, s_{1x} \sin\theta_1 \cos\phi_1 = \omega\sqrt{\mu_2\epsilon_2}\, s_{2x} \sin\theta_2 \cos\phi_2 \tag{25a}$$
$$\omega\sqrt{\mu_1\epsilon_1}\, s_{1y} \sin\theta_1 \sin\phi_1 = \omega\sqrt{\mu_2\epsilon_2}\, s_{2y} \sin\theta_2 \sin\phi_2 \tag{25b}$$

where (ϕ_1, θ_1) define the direction of the incident wave and (ϕ_2, θ_2) the direction of the transmitted wave. The choice

$$\epsilon_1 = \epsilon_2, \quad \mu_1 = \mu_2 \tag{26}$$

and

$$s_{1x} = s_{2x}, \quad s_{1y} = s_{2y} \tag{27}$$

combined with (25a) and (25b) leads to the following result

$$\phi_1 = \phi_2, \quad \theta_1 = \theta_2. \tag{28}$$

Use of (27) and (28) in (23) and (24) leads to the result that $R^{\mathrm{TE}} = R^{\mathrm{TM}} = 0$ for all frequencies and all angles of incidence (except grazing).

Clearly, (27) is an instrumental condition for achieving the reflectionless interface. It can be rewritten in terms of the elements of the tensors $\boldsymbol{\Lambda_1}$ and $\boldsymbol{\Lambda_2}$ making use of (10). The following relations are easily obtained

$$\frac{a_{1x}}{a_{2x}} = \frac{a_{1y}}{a_{2y}} = \frac{a_{2z}}{a_{1z}}. \tag{29}$$

At this point, it is worth noting that, in view of (7), (21) is equivalent to (29).

In summary, let i denote one of the axes in a right-handed Cartesian coordinate system xyz, and j, k the other two axes in the system. The jk-plane interface between two anisotropic media characterized by the tensors $\epsilon_1 \operatorname{diag}\{a_{1x}, a_{1y}, a_{1z}\}, \mu_1 \operatorname{diag}\{a_{1x}, a_{1y}, a_{1z}\}$ and $\epsilon_2 \operatorname{diag}\{a_{2x}, a_{2y}, a_{2z}\}, \mu_2 \operatorname{diag}\{a_{2x}, a_{2y}, a_{2z}\}$, respectively, will be reflectionless for all frequencies and any angle of incidence other than grazing provided that $\epsilon_1 = \epsilon_2, \mu_1 = \mu_2$, and the elements of the tensors satisfy the relation

$$\frac{a_{1j}}{a_{2j}} = \frac{a_{1k}}{a_{2k}} = \frac{a_{2i}}{a_{1i}}. \tag{30}$$

The use of this result in the construction of absorbing PML's for numerical grid truncation is discussed in the next section.

III. Construction of Absorbing PML's

Consider a rectangular volume, Ω, in a linear, homogeneous, isotropic medium of permittivity ϵ and permeability μ. It is assumed that a finite method will be used to model electromagnetic interactions inside this volume, including radiation out of the volume. Toward this objective, it is desirable to surround the volume by PML's developed on the basis of the aforementioned theory with the additional attribute that they dissipate the waves propagating through them. This is highly desirable since, for the purposes of numerical computation, the PML's need be of finite thickness. If sufficient field attenuation is effected by these absorbing PML's, zero field values may be assumed at the end of the PML's, thus effecting simple Dirichlet boundary conditions at the ends of the domain of numerical computation without (hopefully) giving rise to spurious (nonphysical) reflections.

Fig. 1 depicts one fraction of the volume Ω with PML's of finite thickness attached on its outer surface. We distinguish three types of such PML's: face-PML's, edge-PML's and corner PML's.

Face-PML's

These PML's are placed on the six faces of the rectangular volume. Layers PML_x and PML_y in Fig. 1 fall in this category. Consider layer PML_z. This layer is expected to be perfectly matched to the homogeneous medium inside Ω. Let Medium 1 be the medium inside Ω. Thus, $\epsilon_1 = \epsilon, \mu_1 = \mu$, and $a_{1x} = a_{1y} = a_{1z} = 1$. Let Medium 2 be the layer PML_z. According to the results in the previous section, layer

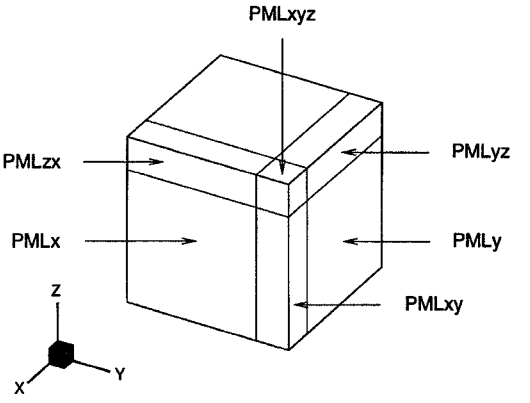

Fig. 1. Classification of the various PML regions.

PML_z will be perfectly matched to the interior medium if $\epsilon_2 = \epsilon, \mu_2 = \mu$ and, from (30),

$$a_{2x} = a_{2y} = w_z, \quad a_{2z} = w_z^{-1}$$

or, in matrix form,

$$[\Lambda^{(z)}] = \operatorname{diag}\{w_z, w_z, w_z^{-1}\}. \tag{31}$$

Note that w_z is not determined at this point. However, as stated earlier, it is desirable to attenuate the wave as it propagates through this face-PML. Using (10) in (15c), the wavenumber in the z direction inside layer PML_z has the form

$$k_{2z} = \omega\sqrt{\mu\epsilon}\sqrt{a_{2x}a_{2y}}\cos\theta = \omega\sqrt{\mu\epsilon}w_z\cos\theta. \tag{32}$$

Thus, the choice

$$s_{2z} = w_z = 1 + \frac{w_z''}{j\omega} \tag{33}$$

leads to a wave variation in the z direction inside the PML_z of the form

$$e^{-jk_{2z}z} = e^{-j\omega\sqrt{\mu\epsilon}z\cos\theta}e^{-w_z''\sqrt{\mu\epsilon}z\cos\theta}.$$

From the second term on the right-hand side of this last equation it becomes clear that the wave is attenuated in the z direction at a rate controlled by w_z''. Finally, taking into account the fact that the elements of the scaling matrix $[G]$ for this face-PML are (from (7))

$$g_{2x} = g_{2y} = 1, \quad g_{2z} = w_z. \tag{34}$$

Maxwell's curl equations inside PML_{Z1} are written in component form as follows:

$$-j\omega\mu w_z H_x = (\nabla \times \boldsymbol{E})_x \tag{35a}$$
$$-j\omega\mu w_z H_y = (\nabla \times \boldsymbol{E})_y \tag{35b}$$
$$-j\omega\mu H_z = w_z(\nabla \times \boldsymbol{E})_z \tag{35c}$$
$$j\omega\epsilon w_z E_x = (\nabla \times \boldsymbol{H})_x \tag{36a}$$
$$j\omega\epsilon w_z E_y = (\nabla \times \boldsymbol{H})_y \tag{36b}$$
$$j\omega\epsilon E_z = w_z(\nabla \times \boldsymbol{H})_z \tag{36c}$$

where $(\nabla \times \boldsymbol{F})_q$ denotes the q component of the curl of field $\boldsymbol{F}, q = x, y, z$.

The construction of the rest of the face-PML's is done in a similar way.

Edge-PML's

These PML's are placed at the twelve edges of the rectangular volume. Fig. 1 depicts three of these edge-PML's, $\mathrm{PML}_{xy}, \mathrm{PML}_{yz}$, and PML_{zx}. Consider the layer PML_{zx}. This PML must be constructed in such a way that it is matched to both face-PML's PML_z and PML_x. In view of (30) and the fact that the [Λ]-matrices of the face-PML's PML_x and PML_z are, respectively, $\mathrm{diag}\{w_x^{-1}, w_x, w_x\}$ and $\mathrm{diag}\{w_z, w_z, w_z^{-1}\}$, this edge-PML should have parameters ϵ and μ, and the elements of its [Λ]-matrix should satisfy the relations

$$\frac{w_z}{a_y} = \frac{w_z^{-1}}{a_z} = \frac{a_x}{w_z} \tag{37a}$$

$$\frac{w_x^{-1}}{a_x} = \frac{w_x}{a_y} = \frac{a_z}{w_x}. \tag{37b}$$

It is straightforward to show that these relations lead to the following [Λ]-matrix for this edge-PML

$$[\Lambda^{(zx)}] = \mathrm{diag}\left\{\frac{w_z}{w_x}, w_z w_x, \frac{w_x}{w_z}\right\} \tag{38}$$

which may also be written in the more convenient form

$$[\Lambda^{(zx)}] = [\Lambda^{(z)}][\Lambda^{(x)}]. \tag{39}$$

Clearly, this last equation is extremely useful since it provides a simple means for constructing the tensors of the rest of the edge-PML's.

From (10), the s parameters for the edge-PML PML_{zx} are easily found to be $s_x = w_x, s_y = 1$, and $s_z = w_z$. Considering that w_z and w_x have already been constructed according to (33), the expressions for k_z and k_x in (15) make it clear that attenuation in both z and x occurs as the wave propagates through this edge-PML. Finally, using the aforementioned values of s parameters and the fact that $g_x = w_x, g_y = 1$ and $g_z = w_z$, Maxwell's equations inside PML_{zx} take the form

$$-j\omega\mu w_z H_x = w_x(\nabla \times \boldsymbol{E})_x \tag{40a}$$

$$-j\omega\mu w_z w_x H_y = (\nabla \times \boldsymbol{E})_y \tag{40b}$$

$$-j\omega\mu w_x H_z = w_z(\nabla \times \boldsymbol{E})_z \tag{40c}$$

$$j\omega\epsilon w_z E_x = w_x(\nabla \times \boldsymbol{H})_x \tag{41a}$$

$$j\omega\epsilon w_z w_x E_y = (\nabla \times \boldsymbol{H})_y \tag{41b}$$

$$j\omega\epsilon w_x E_z = w_z(\nabla \times \boldsymbol{H})_z. \tag{41c}$$

The rest of the edge-PML's are constructed in a similar manner.

Corner-PML's

These PML's are placed at the eight corners of the rectangular volume. One of them, PML_{xyz} is depicted in Fig. 1. Their construction is based on the observation that they need to be matched to the three edge-PML's, $\mathrm{PML}_{xy}, \mathrm{PML}_{yz}$, and PML_{zx}. Application of (30) at the three relevant interfaces leads to the following expression for the [Λ] matrix of the corner-PML

$$[\Lambda^{(xyz)}] = \mathrm{diag}\left\{\frac{w_y w_z}{w_x}, \frac{w_x w_z}{w_y}, \frac{w_x w_y}{w_z}\right\} \tag{42}$$

which may also be written as

$$[\Lambda^{(xyz)}] = [\Lambda^{(x)}][\Lambda^{(y)}][\Lambda^{(z)}].$$

From (10), the s parameters for the corner-PML are found to be $s_x = w_x, s_y = w_y, s_z = w_z$. Thus, with w_x, w_y, and w_z constructed according to (33), the expressions for k_x, k_y and k_z in (15) make it clear that attenuation occurs in all three directions as the wave propagates through the corner-PML. Finally, using the aforementioned values of s parameters and the fact that $g_x = w_x, g_y = w_y$ and $g_z = w_z$, Maxwell's equations inside PML_{xyz} take the form

$$-j\omega\mu w_y w_z H_x = w_x(\nabla \times \boldsymbol{E})_x \tag{43a}$$

$$-j\omega\mu w_z w_x H_y = w_y(\nabla \times \boldsymbol{E})_y \tag{43b}$$

$$-j\omega\mu w_x w_y H_z = w_z(\nabla \times \boldsymbol{E})_z \tag{43c}$$

$$j\omega\epsilon w_y w_z E_x = w_x(\nabla \times \boldsymbol{H})_x \tag{44a}$$

$$j\omega\epsilon w_z w_x E_y = w_y(\nabla \times \boldsymbol{H})_y \tag{44b}$$

$$j\omega\epsilon w_x w_y E_z = w_z(\nabla \times \boldsymbol{H})_z. \tag{44c}$$

IV. GT-PML's for Transient Wave Simulations

The implementation of GT-PML's for numerical grid truncation in transient electromagnetic field simulations is presented in this section. Frequency-domain implementations, as, for example, in frequency-domain finite-elements, have already been discussed in [9]. However, the usefulness of the proposed GT-PML theory lies mainly on the fact that the formulations of (35)–(36), (40)–(41), and (43)–(44) lead to convenient implementation of absorbing PML's for grid truncation in discrete, transient wave simulations, without the requirement for splitting of the field components. The development of the relevant time-dependent form of the equations is presented first, followed by suggested discrete approximations. Only the discrete forms for time derivatives and time integrations are discussed. Discrete forms for the spatial derivatives are dependent on the choice of placement of the field components on the numerical grid and, provided that are effected according to the various popular stable schemes, are irrelevant to the unsplit-field formulation that is the focus of this work.

Consider, first, the case of a face-PML, such as PML_z in Fig. 1. Use of (33) in (35a–c) followed by a Fourier transform back to the time domain results in the following time-dependent form of the equations (assuming that all fields are zero for $t \leq 0$)

$$\frac{\partial H_x}{\partial t} + w_z'' H_x = -\frac{1}{\mu}(\nabla \times \boldsymbol{E})_x \tag{45a}$$

$$\frac{\partial H_y}{\partial t} + w_z'' H_y = -\frac{1}{\mu}(\nabla \times \boldsymbol{E})_y \tag{45b}$$

$$\frac{\partial H_z}{\partial t} = -\frac{1}{\mu}(\nabla \times \boldsymbol{E})_z - \frac{1}{\mu} w_z'' \cdot \int_0^t (\nabla \times \boldsymbol{E})_z \, dt'. \tag{45c}$$

In the above equations all fields are time-dependent quantities. For simplicity, the same symbol used for their phasor form is maintained. Clearly, (45a) and (45b) have the standard

form for wave propagation in a lossy medium with magnetic conductivity $\sigma^* = \mu w_z''$, and their time discretization using either central differencing [12] or exponential differencing [13] is well known. Equation (45c) is different in the sense that a time integral of the z component of the curl of the electric field appears on the right-hand side. This term is interpreted as a time and field-dependent source term. Using the trapezoidal rule for the numerical calculation of this source term one obtains

$$\int_0^{n\Delta t} (\nabla \times \boldsymbol{E})_z \, dt' = \sum_{m=0}^{n-1} (\nabla \times \boldsymbol{E})_z^{(m)} \Delta t + \tfrac{1}{2} (\nabla \times \boldsymbol{E})_z^{(n)} \Delta t \tag{46}$$

where the superscript $^{(q)}$ notation is used to indicate that the specific quantity is calculated at time $t = q\Delta t$. Introducing the quantity

$$F_z^{(n)} = \sum_{m=0}^{n} (\nabla \times \boldsymbol{E})_z^{(m)} \tag{47}$$

and using standard central differencing for the approximation of the time derivative, the semidiscrete form of (45c) is obtained in view of (46) as follows:

$$H_z^{(n+1/2)} = H_z^{(n-1/2)} - \frac{\Delta t}{\mu}\left(1 + \frac{w_z''}{2}\Delta t\right)(\nabla \times \boldsymbol{E})_z^{(n)} - \frac{w_z'' \Delta t^2}{\mu} F_z^{(n-1)}. \tag{48}$$

Clearly, once H_z has been updated, F_z should be updated also using

$$F_z^{(n)} = F_z^{(n-1)} + (\nabla \times \boldsymbol{E})_z^{(n)}. \tag{49}$$

A similar development leads to the time-dependent form and the subsequent development of the semidiscrete approximations of (36a–c). As a matter of fact, duality may be used to derive these equations. Thus, a source term appears on the right-hand side of the update equation for the z component of the electric field, given by

$$\frac{w_z''}{\epsilon} \int_0^t (\nabla \times \boldsymbol{H})_z \, dt'. \tag{50}$$

This source term needs be updated right after E_z has been updated, in a manner similar to the one discussed above.

The time-dependent equations for the face-PML's in the x and y directions and their subsequent semidiscrete approximations are developed in a similar fashion. In summary, for each face-PML two time-dependent source terms are introduced. Their update involves the simple operation indicated in (49).

Next, the equations inside the edge-PML's are examined. Consider, for example, the edge-PML PML_{zx} with equations (40) and (41). In view of the fact that

$$w_x w_z = \left(1 + \frac{w_x''}{j\omega}\right)\left(1 + \frac{w_z''}{j\omega}\right) = 1 + \frac{w_x'' + w_z''}{j\omega} + \frac{w_x'' w_z''}{(j\omega)^2}$$

the time-dependent form of (40a–c) becomes

$$\frac{\partial H_x}{\partial t} + w_z'' H_x = -\frac{1}{\mu}(\nabla \times \boldsymbol{E})_x - \frac{w_x''}{\mu} \int_0^t (\nabla \times \boldsymbol{E})_x \, dt' \tag{51a}$$

$$\frac{\partial H_y}{\partial t} + (w_x'' + w_z'') H_y + w_x'' w_z'' \int_0^t H_y \, dt' = -\frac{1}{\mu}(\nabla \times \boldsymbol{E})_y \tag{51b}$$

$$\frac{\partial H_z}{\partial t} + w_x'' H_z = -\frac{1}{\mu}(\nabla \times \boldsymbol{E})_z - \frac{w_z''}{\mu} \int_0^t (\nabla \times \boldsymbol{E})_z \, dt'. \tag{51c}$$

There are now three source terms present. The ones in (51a) and (51c) are similar with the ones present in the face-PML's, in the sense that they involve time integrals of the specific component of the curl of the electric field. Using the notation

$$\alpha_q^+ = 1 + \frac{\Delta t}{2} w_q'' \tag{52a}$$

$$\alpha_q^- = 1 - \frac{\Delta t}{2} w_q'' \tag{52b}$$

the semidiscrete forms of (51a) and (51c) are

$$H_x^{(n+1/2)} = \frac{\alpha_z^-}{\alpha_z^+} H_x^{(n-1/2)} - \frac{\Delta t \alpha_x^+}{\mu \alpha_z^+} (\nabla \times \boldsymbol{E})_x^{(n)} - \frac{w_x'' \Delta t^2}{\mu \alpha_z^+} \sum_{m=0}^{n-1} (\nabla \times \boldsymbol{E})_x^{(m)} \tag{53a}$$

$$H_z^{(n+1/2)} = \frac{\alpha_x^-}{\alpha_x^+} H_z^{(n-1/2)} - \frac{\Delta t \alpha_z^+}{\mu \alpha_x^+} (\nabla \times \boldsymbol{E})_z^{(n)} - \frac{w_z'' \Delta t^2}{\mu \alpha_x^+} \sum_{m=0}^{n-1} (\nabla \times \boldsymbol{E})_z^{(m)}. \tag{53b}$$

The source term in (51b) is different. It involves the time integral of the magnetic field component that will be updated using this equation. Thus, the time discretization of (51b) at $t = n\Delta t$ will involve the integral

$$\int_0^{n\Delta t} H_y \, dt'.$$

Using the trapezoidal rule for the numerical calculation of this integral, and in view of the fact that the magnetic field is sampled in time at points $(i + 1/2)\Delta t, i = 1, 2, \cdots$, one obtains

$$\int_0^{n\Delta t} H_y \, dt' = \sum_{m=0}^{n-1} H_y^{(m+1/2)} \Delta t.$$

This last expression, along with the definition of the following quantities

$$\gamma_{pq}^+ = 1 + \frac{\Delta t}{2}(w_p'' + w_q'') \tag{54a}$$

$$\gamma_{pq}^- = 1 - \frac{\Delta t}{2}(w_p'' + w_q'') \tag{54b}$$

lead to the following compact form for the semidiscrete approximation of (51b)

$$H_y^{(n+1/2)} = \frac{\gamma_{zx}^-}{\gamma_{zx}^+} H_y^{(n-1/2)} - \frac{\Delta t}{\mu \gamma_{zx}^+} (\nabla \times \boldsymbol{E})_y^{(n)} - \frac{w_x'' w_z'' \Delta t^2}{\gamma_{zx}^+} \sum_{m=0}^{(n-1)} H_y^{(m+1/2)}. \quad (55)$$

The semidiscrete approximations of (41a–c) can be obtained from (53a), (53b), and (55) using duality. Clearly, a total of six source terms are required in an edge-PML. The semidiscrete approximations of Maxwell's equations in the rest of the edge-PML's are developed in a similar fashion.

Finally, the development of the semidiscrete forms for Maxwell's equations in the corner-PML's is undertaken. A direct inspection of (43a)–(43c) and (44a)–(44c), and use of the experience gained from the development of the edge-PML's makes it clear that two time integrations (sources) will be associated with update of each scalar component. Using (52) and (54) leads to the following compact form for the semidiscrete approximation of (43a)–(43c)

$$H_x^{(n+1/2)} = \frac{\gamma_{yz}^-}{\gamma_{yz}^+} H_x^{(n-1/2)} - \frac{\Delta t \alpha_x^+}{\mu \gamma_{yz}^+} (\nabla \times \boldsymbol{E})_x^{(n)} - \frac{w_x'' \Delta t^2}{\mu \gamma_{yz}^+} \sum_{m=0}^{(n-1)} (\nabla \times \boldsymbol{E})_x^{(m)} - \frac{w_y'' w_z'' \Delta t^2}{\gamma_{yz}^+} \sum_{m=0}^{(n-1)} H_x^{(m+1/2)} \quad (56a)$$

$$H_y^{(n+1/2)} = \frac{\gamma_{zx}^-}{\gamma_{zx}^+} H_y^{(n-1/2)} - \frac{\Delta t \alpha_y^+}{\mu \gamma_{zx}^+} (\nabla \times \boldsymbol{E})_y^{(n)} - \frac{w_y'' \Delta t^2}{\mu \gamma_{zx}^+} \sum_{m=0}^{(n-1)} (\nabla \times \boldsymbol{E})_y^{(m)} - \frac{w_x'' w_z'' \Delta t^2}{\gamma_{zx}^+} \sum_{m=0}^{(n-1)} H_y^{(m+1/2)} \quad (56b)$$

$$H_z^{(n+1/2)} = \frac{\gamma_{xy}^-}{\gamma_{xy}^+} H_z^{(n-1/2)} - \frac{\Delta t \alpha_z^+}{\mu \gamma_{xy}^+} (\nabla \times \boldsymbol{E})_z^{(n)} - \frac{w_z'' \Delta t^2}{\mu \gamma_{xy}^+} \sum_{m=0}^{(n-1)} (\nabla \times \boldsymbol{E})_z^{(m)} - \frac{w_x'' w_y'' \Delta t^2}{\gamma_{xy}^+} \sum_{m=0}^{(n-1)} H_z^{(m+1/2)}. \quad (56c)$$

The semidiscrete approximations of (44a)–(44c) can be obtained from (56a)–(56c) using duality.

V. Numerical Experiments

In order to validate numerically the derived time-dependent source implementation of the anisotropic, perfectly matched medium, the numerical experiment of [14] was attempted in three dimensions. A z-directed point source at the center of a $50 \times 50 \times 51$-cell domain, Ω_N, was excited by a smooth compact pulse. The domain of computation was terminated

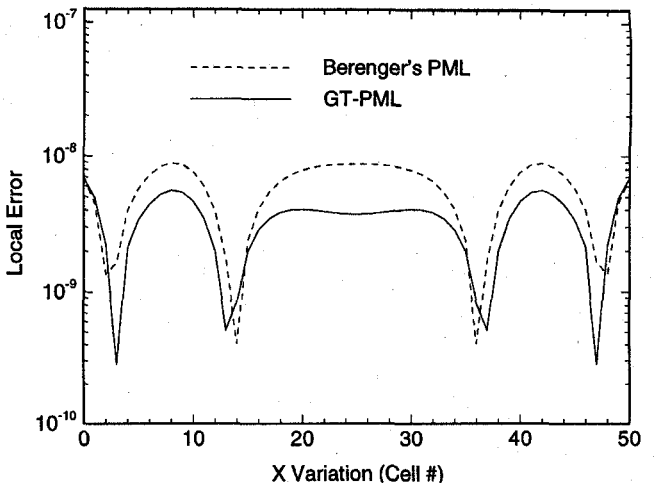

Fig. 2. Local error in $E_z(x, 0, 0)$ within a $50 \times 50 \times 51$-cell FDTD grid with a pulsed *Member, IEEE*z-directed point source at its center ($t = 100\Delta t$). Grid truncation was effected using Berenger's split-field PML (dashed line), as well as the proposed unsplit-field GT-PML (solid line). Eight-cell layers were used in both cases.

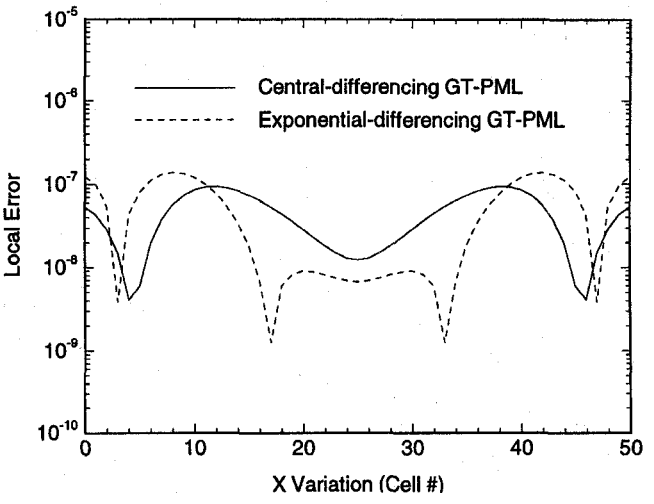

Fig. 3. Local error in $E_z(x, 0, 0)$ within a $50 \times 50 \times 51$-cell FDTD grid with a pulsed z-directed point source at its center ($t = 100\Delta t$). Exponential-differencing implementation (dashed line) is compared with central-differencing implementation (solid line) for four-cell GT-PML's.

by either Berenger's PML backed by perfect electric conductors, or by the proposed GT-PML also backed by perfect electric conductors. The benchmark FDTD solution, with zero truncation boundary reflections, was obtained by simulating radiation by the aforementioned point source in a much larger domain, Ω_L, centered at the point source, discretized by a finite-difference grid of same cell size as that for Ω_N, and with truncation boundaries placed sufficiently far away to provide for causal isolation for all points in Ω_N over the time interval used for the comparisons.

The error due to numerical reflections caused by the presence of the conductor-backed PML's was obtained by subtracting at each time step the field at any grid point inside Ω_N from the field at the corresponding point in Ω_L. Fig. 2 compares the local error for $E_z(x, 0, 0)$ as observed at time step 100 for the standard Berenger's PML (dashed-line) to

that for the proposed GT-PML (solid line). In both cases, eight-element PML's were used with quadratic variation in the conductivities (for Berenger's PML) or, equivalently the quantities w_x'', w_y'', w_z'' (for the GT-PML's). Their maximum value was chosen for theoretical reflection coefficient of 10^{-5} at normal incidence. The effectiveness of the proposed GT-PML is clearly demonstrated.

It is pointed out that in the aforementioned implementation of the GT-PML exponential differencing was not used. Indeed, the semidiscrete equations of the previous section were developed using the standard central differencing approach familiar from the time discretization of Maxwell's equations in lossy media. Of course, exponential differencing may be used also if so desired. Fig. 3 compares the local error for $E_z(x, 0, 0)$ as observed at time step 100 for GT-PML with exponential differencing (dashed-line) to that for GT-PML with central differencing (solid line). A four-element PML was used. The variation in the quantities w_x'', w_y'', w_z'' was quadratic with maximum value such that the theoretical reflection coefficient was 10^{-5} at normal incidence. For both implementation the performance of the PML remains essentially the same.

In order to perform a comparison of Berenger's PML and GT-PML requirements for memory and CPU, we consider a cubical domain N cells on each side. An M-cell PML is used on each one of the faces of the domain. Berenger's PML utilizes $10(N - 2M)^2M$ variables per face-PML, $12(N - 2M)M^2$ variables per edge-PML, and $12M^3$ variables per corner-PML, for a total of $60(N - 2M)^2M + 144(N - 2M)M^2 + 96M^3$ variables. GT-PML utilizes $8(N - 2M)^2M$ variables per face-PML, $12(N - 2M)M^2$ variables per edge-PML, and $18M^3$ variables per edge-PML, for a total of $48(N - 2M)^2M + 144(N - 2M)M^2 + 144M^3$ variables. Thus Berenger's PML formulation utilizes $12NM(N - 4M)$ variables more than the GT-PML, where $N > 4M$ is assumed. Considering that typical values of M are in the order of ten, and that typical simulations involve domains that span several wavelengths on each side, the above inequality is expected to hold for most practical applications. Therefore, the GT-PML formulation provides for significant storage savings over Berenger's PML formulation. More specifically, let us consider the case of an FDTD grid with a resolution of $Q = 32$ cells per wavelength. If the cubical domain is L wavelengths on each side and $M = 8 = Q/4$, the savings in memory are $3L(L - 1)Q^3$. For values of $L \geq 10$, the total number of variables used in the original PML formulation is approximately $12L^2Q^3$. Consequently, the GT-PML formulation results in memory savings of $\sim$25% over the original PML formulation.

With regards to the comparison of the CPU time required by the GT-PML to that for Berenger's PML, the following estimates are relevant. For an FDTD cell in a face-PML, Berenger's formulation requires 44 additions/subtractions and 22 multiplications/divisions for the update of the electric and magnetic fields in the cell per time step, while the GT-PML requires 36 additions/subtractions and 20 multiplications/divisions. For an FDTD cell in an edge-PML, Berenger's formulation requires 56 additions/subtractions and 36 multiplications/divisions for the update of the electric and magnetic fields in the cell per time step, while the GT-PML requires 54 additions/subtractions and 36 multiplications/divisions. Finally, for an FDTD cell in a corner-PML, Berenger's formulation requires 60 additions/subtractions and 48 multiplications/divisions for the update of the electric and magnetic fields in the cell per time step, while the GT-PML requires 78 additions/subtractions and 48 multiplications/divisions. With the observation that it is the face-PML's and edge-PML's that dominate the total number of variables in the PML region, the above numbers indicate that the GT-PML is computationally more efficient that the original Berenger's formulation.

VI. Conclusion

In conclusion, a GT-PML has been presented to facilitate the systematic development of anisotropic media PML's that can be implemented for the truncation of FDTD grids without any splitting of the fields. The frequency dependence of the primitivities and permeabilities in the diagonal tensors that characterize the anisotropic PML's lead to the introduction of field-dependent source terms in the time-dependent form of Maxwell's equations inside the PML regions.

The discrete forms of all relevant equations for the numerical implementation of the proposed anisotropic absorbers have been presented. Numerical examples have been used to demonstrate the numerical stability of the proposed formulation and compare its performance to that of the original Berenger's formulation. The performance of the GT-PML is found to be comparable to Berenger's formulation; however, GT-PML is shown to be computationally less expensive than Berenger's formulation, requiring both less memory and less CPU time for its implementation.

References

[1] J. P. Berenger, "A perfectly matched layer for the absorption of electromagnetic waves," *J. Comput. Phys.*, vol. 114, pp. 185–200, Oct. 1994.

[2] W. C. Chew and W. H. Weedon, "A 3-D perfectly matched medium from modified Maxwell's equations with stretched coordinates," *Microwave Opt. Technol. Lett.*, pp. 599–604, Sept. 1994.

[3] D. S. Katz, E. T. Thiele, and A. Taflove, "Validation and extension to three dimensions of the Berenger PML absorbing boundary condition for FDTD meshes," *IEEE Microwave Guided Wave Lett.*, vol. 4, pp. 268–270, Aug. 1994.

[4] C. E. Reuter, R. M. Joseph, E. T. Thiele, D. S. Katz, and A. Taflove, "Ultrawideband absorbing boundary condition for termination of waveguiding structures in FDTD simulations," *IEEE Microwave Guided Wave Lett.*, vol. 4, pp. 344–346, Oct. 1994.

[5] M. A. Gribbons, W. P. Pinello, and A. C. Cangellaris, "A stretched coordinate technique for numerical absorption of evanescent and propagating waves in planar waveguiding structures," *IEEE Trans. Microwave Theory Tech*, vol. 43, pp. 2883–2889, Dec. 1995.

[6] A. Bahr, A. Lauer, and I. Wolff, "Application of the PML absorbing boundary condition to the FDTD analysis of microwave circuits," in *IEEE MTT-S Int. Microwave Symp. Dig.*, 1995, pp. 27–30.

[7] C. M. Rappaport, "Perfectly matched absorbing boundary conditions based on anisotropic lossy mapping of space," *IEEE Microwave Guided Wave Lett.*, vol. 5, pp. 90–92, Mar. 1995.

[8] R. Mittra and Ü. Pekel, "A new look at the perfectly matched layer (PML) concept for the reflectionless absorption of electromagnetic waves," *IEEE Microwave Guided Wave Lett.*, vol. 5, pp. 84–86, Mar. 1995.

[9] Z. S. Sacks, D. M. Kingsland, R. Lee, and J. F. Lee, "A perfectly matched anisotropic absorber for use as an absorbing boundary condition," *IEEE Trans. Antennas Propagat.*, vol. 43, pp. 1460–1463, Dec. 1995.

[10] J. C. Veihl and R. Mittra, "An efficient implementation of Berenger's perfectly matched layer (PML) for finite difference time domain mesh truncation," *IEEE Microwave Guided Wave Lett.*, vol. 6, pp. 94–96, Feb. 1996.
[11] J. Fang and Z. Wu, "Generalized perfectly matched layer—An extension of Berenger's perfectly matched layer boundary condition," *IEEE Microwave Guided Wave Lett.*, vol. 5, pp. 451–453, Dec. 1995.
[12] J. P. Berenger, "Perfectly matched layer for the FDTD solution of wave-structure interaction problems," *IEEE Trans. Antennas Propagat.*, vol. 44, pp. 110–117, Jan. 1996.
[13] L. Zhao and A. C. Cangellaris, "A general approach for the development of unsplit-field time-domain implementations of perfectly matched layers for FDTD grid truncation," *IEEE Microwave Guided Wave Lett.*, vol. 6, pp. 209–211, May 1996.
[14] T. G. Moore and J. G. Blaschak, A. Taflove, and G. A. Kriegsmann, "Theory and application of radiation boundary operators," *IEEE Trans. Antennas Propagat.*, vol. 36, pp. 1797–1812, Dec. 1988.
[15] S. D. Gedney, "An anisotropic PML absorbing media for the FDTD simulation of fields in lossy and dispersive media," *Electromagn.*, vol. 16, pp. 399–415, July 1996.

Li Zhao (M'94) received the B.S, M.S., and Ph.D. degrees in electrical engineering from Southeast University, China, in 1983, 1988 and 1993, respectively. During the period 1983–1986, he was with the Electronics Research Institute of Nanjing Institute of Technology.

In 1988, he joined the Department of Electronic Engineering at Southeast University, China, where he was Associate Professor. Since 1995, he has been with the Department of Electrical and Computer Engineering at the University of Arizona as Visiting Research Engineer. His research interests are in computational electromagnetics, microwave engineering, and the numerical simulation of high-speed digital circuit. He has published over 30 journal and international conference papers on the aforementioned areas of research.

Andreas C. Cangellaris (M'86), for a photograph and biography, see this issue, p. 2535.